



## Mechanical exfoliation of two-dimensional materials

Enlai Gao<sup>a</sup>, Shao-Zhen Lin<sup>a,b</sup>, Zhao Qin<sup>c,d</sup>, Markus J. Buehler<sup>c,d</sup>, Xi-Qiao Feng<sup>a,b</sup>, Zhiping Xu<sup>a,e,\*</sup>



<sup>a</sup> Applied Mechanics Laboratory, Department of Engineering Mechanics and Center for Nano and Micro Mechanics, Tsinghua University, Beijing 100084, China

<sup>b</sup> Institute of Biomechanics and Medical Engineering, Tsinghua University, Beijing 100084, China

<sup>c</sup> Laboratory for Atomistic and Molecular Mechanics (LAMM), Department of Civil and Environmental Engineering, Massachusetts Institute of Technology, 77 Massachusetts Ave., Cambridge, MA 02139, USA

<sup>d</sup> Center for Computational Engineering, Massachusetts Institute of Technology, 77 Massachusetts Ave., Cambridge, MA 02139, USA

<sup>e</sup> Applied Mechanics and Structure Safety Key Laboratory of Sichuan Province, School of Mechanics and Engineering, Southwest Jiaotong University, Chengdu 611756, China

### ARTICLE INFO

#### Article history:

Received 29 January 2018

Revised 27 February 2018

Accepted 19 March 2018

Available online 24 March 2018

#### Keywords:

Two-dimensional materials

Mechanical exfoliation

Peeling

Tearing

Atomistic simulations

### ABSTRACT

Two-dimensional materials such as graphene and transition metal dichalcogenides have been identified and drawn much attention over the last few years for their unique structural and electronic properties. However, their rise begins only after these materials are successfully isolated from their layered assemblies or adhesive substrates into individual monolayers. Mechanical exfoliation and transfer are the most successful techniques to obtain high-quality single- or few-layer nanocrystals from their native multi-layer structures or their substrate for growth, which involves interfacial peeling and intralayer tearing processes that are controlled by material properties, geometry and the kinetics of exfoliation. This procedure is rationalized in this work through theoretical analysis and atomistic simulations. We propose a criterion to assess the feasibility for the exfoliation of two-dimensional sheets from an adhesive substrate without fracturing itself, and explore the effects of material and interface properties, as well as the geometrical, kinetic factors on the peeling behaviors and the torn morphology. This multi-scale approach elucidates the microscopic mechanism of the mechanical processes, offering predictive models and tools for the design of experimental procedures to obtain single- or few-layer two-dimensional materials and structures.

© 2018 Elsevier Ltd. All rights reserved.

## 1. Introduction

Two-dimensional (2D) materials, including graphene and its derivatives, transition metal dichalcogenides (TMDs), phosphorene, 2D boron, silica mono- and bi-layers have drawn much attention because of their unique structural, mechanical and optoelectronic properties that are uncovered recently (Butler et al., 2013). Promising applications such as the opto-electro-mechanical devices and functional nanostructured membranes have been fabricated and widely explored in practice (Pumera et al., 2010; Shao et al., 2010; Wei et al., 2014). However, their rise begins only after being successfully cleaved from their layered assemblies into high-quality monolayer samples. Mechanical exfoliation that was used in the original work to

\* Corresponding author.

E-mail address: [xuzp@tsinghua.edu.cn](mailto:xuzp@tsinghua.edu.cn) (Z. Xu).

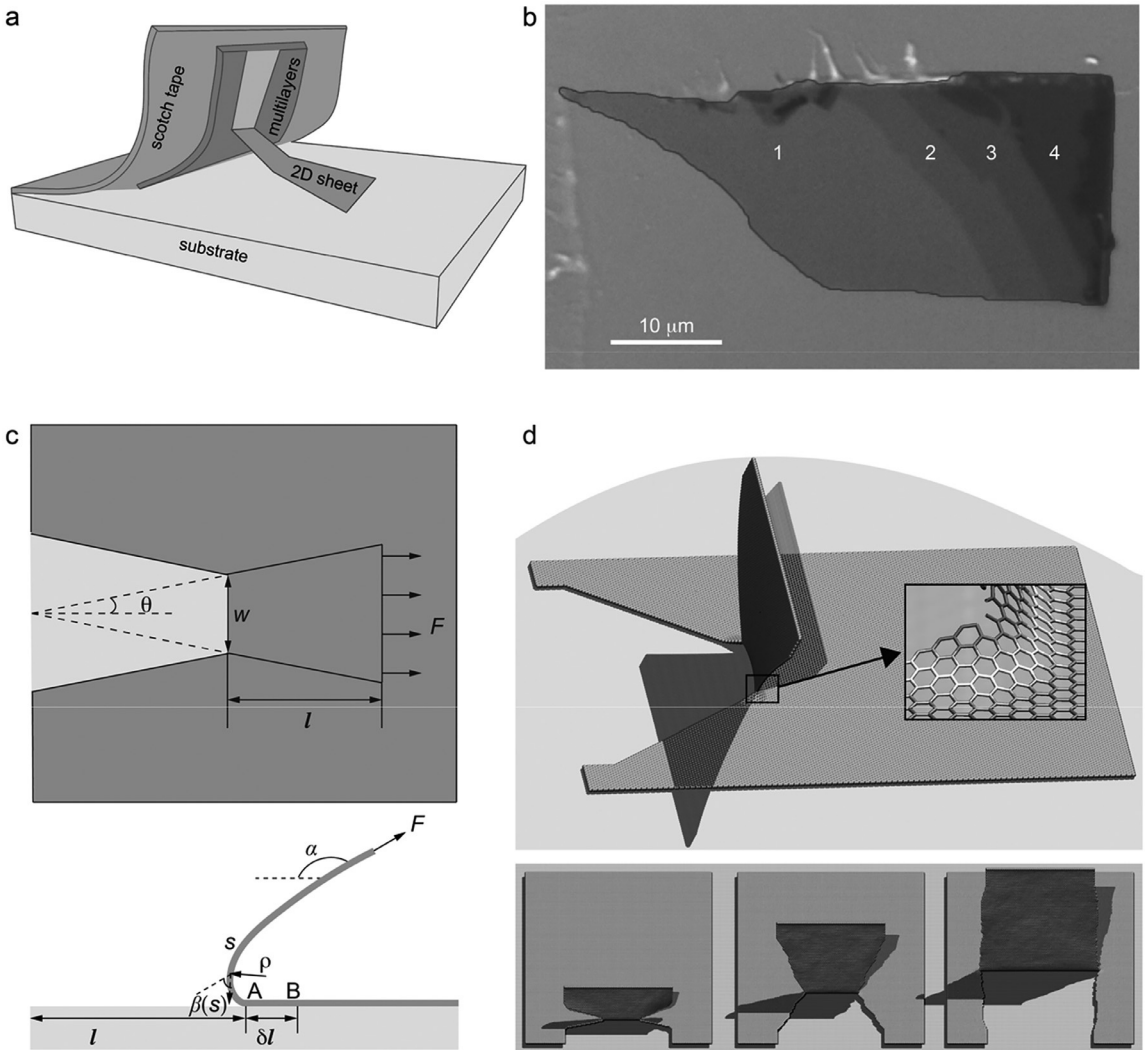


**Fig. 1.** (a) Schematic illustration of the mechanical exfoliation process, where a peeling force is applied by the adhesive substrate or tape, and the peeled sheet detaches during the peeling process. (b) The optical image of exfoliated graphene monolayer and multilayers (the number of layers is denoted by the numbers). (c) A 2D sheet peeled off from an adhesive substrate (top and side views). (d) Detailed views of the peeling front and edges, where the width  $w$  changes with peeling. The results are obtained from our CGMD simulations.

isolate graphene is one of the most successful techniques for this aim (Novoselov et al., 2005; Novoselov et al., 2004). In addition to preparing 2D materials in a monolayer or few-layer form (Allen et al., 2010; Varoon et al., 2011; Yi and Shen, 2015), their successful transfer (Kim et al., 2013) from the host substrate for growth to another one is also a key technology under development for the applications of 2D materials (Allen et al., 2009; Chen et al., 2013) and the construction of van der Waals heterostructures where 2D sheets are stacked in a specified layered order (Geim and Grigorieva, 2013; Kotov and Weiss, 2014). To successfully exfoliate or transfer atomic-thin membranes, theoretical models for the mechanical design are desired. To be specific, as a peeling force is applied to the single- or few-atom-thick sheets through their attachment to the stamp material such as a scotch tape, one could cleave the sheet from a substrate. Morphology of the exfoliated samples shows that the sheets are usually torn in part during peeling, with cracks nucleation and propagation along the sheet-substrate interface for successful exfoliation, and within the materials by fracturing the sheet into pieces (Fig. 1a), which can be rationalized into a forced peeling process as illustrated in Fig. 1c, where the mode selection between peeling and tearing is determined by the material properties, peeling geometry and kinetics.

The theory of mechanical peeling for linear elastic films adhered to a rigid substrate was firstly formulated by Rivlin (1944), and was later generalized to elastic-plastic materials by Aravas, Hutchinson and co-workers (Kim and Aravas, 1988; Tvergaard and Hutchinson, 1992; Wei and Hutchinson, 1998). Tearing of the films was overlooked in these models, however, by assuming that only peeling is activated in the process. It was reported that the film adhered to the substrate

could deform and fracture while being peeled off using adhesive tapes, leading to quasi-perfect triangular tears (Hamm et al., 2008). Follow-up experimental studies extended the exploration to substrates with curved surfaces (Kruglova et al., 2011). Due to their single- or few-atom-thick nature, the 2D sheets could be fragile under peeling, and the control of exfoliated geometry is technically challenging considering the interplay between material properties and the peeling setup. Numerical simulations have been carried out to elucidate microscopic mechanisms of the mechanical process. In earlier work some authors of this paper studied the conditions for a tearing process to produce tapered graphene nanoribbons (Sen et al., 2010). Qin et al. modeled the peeling of silicene sheets from a silver substrate and find that the triangular geometry of torn sheets is robust against change in the tearing angle (Qin et al., 2015). Despite these earlier results reported in the literature, a predictive theory and model that can correlate the peeling and tearing behaviors to the material properties and peeling setup (geometry, speed) is still lacking, which prevents from generalizing mechanical exfoliation techniques to the wide and increasing spectrum of 2D materials.

Compared to their macroscopic counterparts, 2D materials feature many unique structural and mechanical properties (Blees et al., 2015; Xu, 2016). Their single- or few-atom-layer structures leads to low out-of-plane bending stiffness,  $D$ , on the order of 1 eV (Gao and Xu, 2015; Huang et al., 2006; Koskinen and Kit, 2010; Kudin et al., 2001; Zhang et al., 2011), and high in-plane tensile stiffness  $K$  (on the order of 100 N/m) and 2D tensile strength  $\sigma_s$  (on the order of 10 N/m) (Li, 2012; Liu et al., 2007). As a result, the Föppl-von Karman number, defined as  $FvK=KL^2(1-\nu^2)/D$ , could be high, on the order of  $10^{10}$ – $10^{11}$  for 2D sheets with lateral size of  $L=10\mu\text{m}$ , while the thin-shell thickness  $t_s=[12(1-\nu^2)D/K]^{1/2}$  is small, on the order of 0.1–1 nm (Gao and Xu, 2015). The amplitudes of these two characteristic numbers demonstrate the superior flexibility of 2D materials under mechanical or thermal perturbation.

On the other hand, the interfaces between 2D materials and the substrate are usually mediated through a wide range of interactions ranging from chemical bonds, van der Waals to electrostatic interactions, which could be tuned by the chemistry of interfaces. The interfacial adhesive strength is usually in the range of 0.1–10 N/m, comparable with the in-plane tensile strength which is 1–10 N/m (Table S1). This is in stark contrast with the adhesive interface of scotch tape, where in-plane tensile strength of the film,  $10^3$ – $10^4$  N/m, is significantly higher than the interfacial strength 10<sup>2</sup> N/m (Table S2). Therefore, while being exfoliated from an adhesive substrate, fracture of the 2D sheets can be activated, and a predictive model should be developed to devise the experimental procedures, towards high quality and yield control. To achieve this, the key roles of material properties, peeling geometry, force amplitude and rate should be discussed for optimal design of the process.

In this work, we address these issues by analyzing and simulating the mechanical exfoliation process of representative 2D materials from an adhesive substrate. The theoretical model is introduced in Section 2, followed by atomistic simulations based studies, with the detailed methodology described in Section 3. The results not only verify predictions from the analytical model, but also yield a few key findings that complements the theory, as discussed in Section 4 with focus on the impact in designing mechanical exfoliation and transfer processes for 2D materials. Section 5 concludes the current work.

## 2. Theory for the peeling and tearing processes

Considering the mechanical exfoliation process of a 2D sheet from a flat and rigid substrate, with a geometry illustrated in Fig. 1c, the elastic energy of the sheet is

$$U_E = U_B + U_T \quad (1)$$

where the two terms  $U_B$  and  $U_T$  arise from the bending deformation of the ridge and stretching deformation of the sheet (Fig. 1c). In a displacement-controlled peeling experiment where the upper edge of the sheet is pulled upward, the first-order variation of the total energy  $U$  is

$$\delta U = (\partial_w U_E)_l \delta w + (\partial_l U_E)_w \delta l + 2\gamma_s t_s \delta s + \gamma_i w \delta l - \left[ F(1 - \cos\alpha) + \frac{F^2}{Kw} \right] \delta l \quad (2)$$

where  $\sin\theta = -\delta_w/2\delta s$  and  $=\cos\theta = \delta l/\delta s$ . We here introduce  $\gamma_s$  as the cleavage energy density of the 2D sheet which corresponds to the cracking process leaving a pair of fresh edges, and  $\gamma_i$  as the interfacial energy density between the 2D sheet and the substrate.  $l$  is the distance that peeling front travels,  $s$  and  $w$  are the length and width of cracks created by peeling,  $\alpha$  and  $\theta$  are the peeling and tearing angles, and  $F$  is the amplitude of peeling force (Fig. 1c). It should be noted here that the thickness of 2D materials was defined through thin-shell thickness  $t_s$  (Gao and Xu, 2015; Huang et al., 2006; Kudin et al., 2001). The in-plane tensile stiffness  $K=Yt_s$ , where  $Y$  is the Young's modulus of 2D materials. The r.h.s. terms of Eq. (2) include the variation of elastic strain energy, edge-cleavage energy, the sheet-substrate adhesion and work done by the external peeling force. The last term includes  $F(1 - \cos\alpha)\delta l$  resulted from the movement of loading point where the sheet is considered to be inextensible, and a nonlinear elastic term  $\frac{F^2}{Kw}\delta l$  for the stretched region AB (Fig. 1c).

The condition of mechanical equilibrium can then be derived from  $\partial U/\partial s=0$  as

$$(\partial_l U_E)_w \cos\theta = 2(\partial_w U_E)_l \sin\theta - 2\gamma_s t_s - \gamma_i w \cos\theta + \left[ F(1 - \cos\alpha) + \frac{F^2}{Kw} \right] \cos\theta \quad (3)$$

and the criterion for the maximum energy release rate is  $\partial_\theta(\partial U/\partial s)=0$ , or

$$(\partial_l U_E)_w \sin\theta = -2(\partial_w U_E)_l \cos\theta - \gamma_1 w \sin\theta + \left[ F(1 - \cos\alpha) + \frac{F^2}{Kw} \right] \sin\theta \quad (4)$$

Eqs. (3) and (4) can be further simplified into

$$F(1 - \cos\alpha) + \frac{F^2}{Kw} = (\partial_l U_E)_w + 2\gamma_s t_s \cos\theta + \gamma_1 w \quad (5)$$

$$\sin\theta = \frac{(\partial_w U_E)_l}{\gamma_s t_s} \quad (6)$$

which constitute the governing equations for the mechanical exfoliation of the 2D sheet. To solve Eqs. (5) and (6), one should first derive the analytical expressions for bending and stretching energy terms of the sheet.

### 2.1. Bending of the 2D sheet

We first calculate the bending energy of a 2D sheet under the peeling force  $F$  by assuming that it can be described mathematically using an inextensible planar curve. Here we use the curvilinear coordinates  $(s, \beta)$  where  $s$  is the curvilinear abscissa and  $\beta$  is the angle measuring the local tangent to the curve with respect to the peeling force direction (Fig. 1c). Noting that the curvature  $\kappa(s)$  is the rate of change in  $\beta(s)$ , we have  $\kappa(s) = d\beta/ds$ . The bending momentum  $M(s) = Dw\kappa(s)$  can then be written as

$$Dw \frac{d\beta}{ds} = F \int_0^s \sin \beta ds \quad (7)$$

It should be noted that bending is localized at the ridge of peeling front that connects the flap to the substrate. Accordingly, one could assume width of bent sheet is a constant in this ridge, while outside the ridge we have  $\beta \approx 0$  (Kruglova et al., 2011; Hamm et al., 2008). Therefore, taking the derivation of both sides in Eq. (7), one arrives at

$$\frac{d^2\beta}{ds^2} = \frac{F \sin \beta}{Dw} \quad (8)$$

Using  $\kappa(s) = d\beta/ds$ , we have

$$\kappa(s) \frac{d\kappa(s)}{d\beta} = \frac{F \sin \beta}{Dw} \quad (9)$$

Integrating Eq. (9) with the boundary condition  $p|_{\beta=0}=0$  leads to

$$\kappa^2(s) = \frac{2F(1 - \cos\beta)}{Dw} \quad (10)$$

Thus the curvature is

$$\frac{d\beta}{ds} = \sqrt{\frac{2F(1 - \cos\beta)}{Dw}} \quad (11)$$

and the bending energy of a 2D sheet is

$$U_B = \frac{1}{2} \int_0^s Dw\kappa(s)^2 ds = \sqrt{2FDw} \left( \sqrt{2} - \frac{\sin\alpha}{\sqrt{1 - \cos\alpha}} \right) \quad (12)$$

which does not depend on the torn sheet as bending is localized.

### 2.2. Stretching of the 2D sheet

By assuming that the material is isotropic and linearly elastic, which is reasonable for most 2D materials except for the black phosphorus with non-hexagonal lattice structures (Table S1), the stretching energy of a 2D sheet is calculated by integrating the strain energy density over the length  $l$ , that is

$$U_T = \int_0^l \frac{F^2}{2Kw(x)} dx = \frac{fF^2 l}{Kw} \quad (13)$$

A dimensionless shape factor  $f$  is introduced in Eq. (13) to measure the dependence of stretching energy of torn sheet on the shape of torn sheet, which is 0.5 for a rectangular sheet.

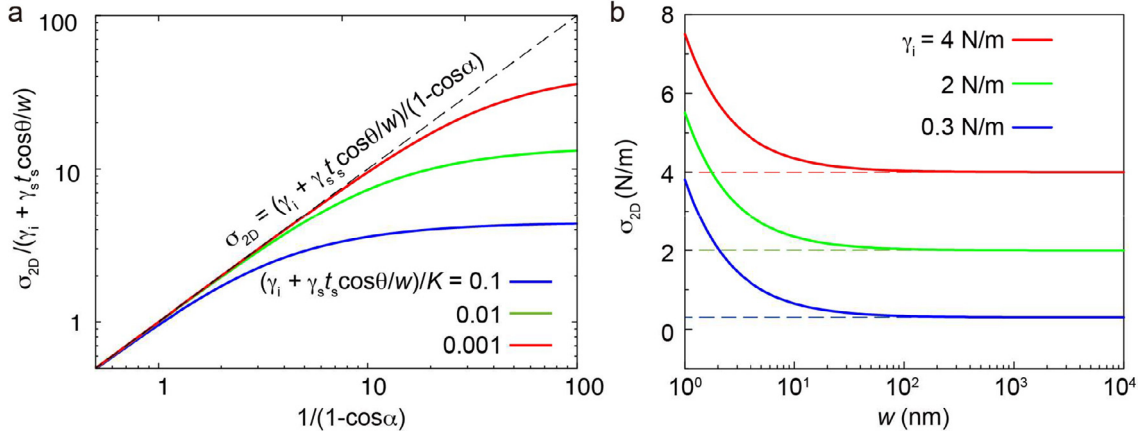


**Fig. 2.** The 2D peeling stress  $\sigma_{2D}$  predicted from Eq. (14) as a function of  $(1 - \cos\alpha)^{-1}$  or  $w$ . The results in panel (a) demonstrate significance of the nonlinear term of  $\sigma_{2D}$  at a small peeling angle and a high peeling stress, while data in panel (b) shows that the effect of the edge fracture term on  $\sigma_{2D}$  stress is negligible for large  $w$ .

### 2.3. Governing equations for the torn geometry

With Eqs. (5), (12) and (13), the generalized governing equation can be derived as

$$F(1 - \cos\alpha) + \frac{(1 - f)F^2}{Kw} = \gamma_i w + 2\gamma_s t_s \cos\theta \quad (14)$$

where the linear and nonlinear terms of the peeling force  $F$  on the left balance the interfacial adhesion  $\gamma_i w$  and the edge cleavage energy  $2\gamma_s t_s \cos\theta$ . It should be remarked here that the formula can be reduced to the equation  $F(1 - \cos\alpha) + F^2/2Kw = \gamma_i w$  given by Kendall (1975) where edge cleavage is excluded in the peeling processes, and  $F(1 - \cos\alpha) = \gamma_i w + 2\gamma_s t_s \cos\theta$  derived by Hamm et al. (2008) where the nonlinear term is not considered in studying tape peeling, and  $F(1 - \cos\alpha) = \gamma_i w$  proposed by Rivlin (1944) if both the edge cleavage and the nonlinear term are neglected. Moreover, as bending is localized at the ridge and the bending energy is independent on the distance  $l$  the peeling front travels (Kruglova et al., 2011; Hamm et al., 2008), one can find from Eqs. (5), (12) and (14) that  $U_B$  has no contribution to  $F$ . However, it should be noted that this conclusion is valid only for the steady-state stage of peeling, while the bending could influence on the peeling force in the initial stage of peeling (Peng and Chen, 2015).

For mechanical exfoliation of 2D materials, considering the fact that the value of  $\gamma_i w$  is much larger than  $\gamma_s t_s$  and the high in-plane stiffness (typical values are  $\gamma_i \approx 0.3 \text{ J/m}^2$ ,  $w \approx 1 - 10 \mu\text{m}$ ,  $\gamma_s t_s \approx 2.2 \text{ eV/\AA}$ , and  $K = 345 \text{ N/m}$  for graphene), the contribution of the edge cleavage term for the peeling force can be neglected, and the nonlinear term is significant only in the condition when  $\alpha$  is very small (Fig. 2). Hence the peeling force is mainly applied to balance the interfacial adhesion, which can be approximated as  $F \approx \gamma_i w/(1 - \cos\alpha)$ , and with Eqs. (12) and (13), we have

$$U_T = \frac{f\gamma_i^2 w l}{K(1 - \cos\alpha)^2} \quad (15)$$

$$U_B = \sqrt{\gamma_i D} w \left( \frac{2}{\sqrt{1 - \cos\alpha}} - \frac{\sqrt{2} \sin\alpha}{1 - \cos\alpha} \right) = \sqrt{\gamma_i D} w g(\alpha) \quad (16)$$

Specifically, one can further expand  $g(\alpha)$  into the Taylor series as

$$g(\alpha) = \frac{2}{\sqrt{1 - \cos\alpha}} - \frac{\sqrt{2} \sin\alpha}{1 - \cos\alpha} = \frac{\sqrt{2}}{4} \alpha + \frac{\sqrt{2}}{192} \alpha^3 + O(\alpha^5) \quad (17)$$

and the 1st- and 3rd-order approximations of the bending energy are

$$U_B = \frac{\sqrt{2\gamma_i D} w}{4} \alpha + \frac{\sqrt{2\gamma_i D} w}{192} \alpha^3 \quad (18a)$$

$$U_B = \frac{\sqrt{2\gamma_i D} w}{4} \alpha + \frac{\sqrt{2\gamma_i D} w}{192} \alpha^3 \quad (18b)$$

respectively. Kruglova et al. (Kruglova et al., 2011) derived a linear relation between the bending energy and  $\alpha$  for the tearing process based on the assumption that the peeling force induces localized deformation at the ridge with an uniform

curvature, connecting the flap sheet and substrate. The form of bending energy derived by Kruglova is actually the 1st-order approximation of Eq. (16). Compared to the exact solution obtained within the entire range of  $\alpha$  in  $[0, \pi]$ , the errors introduced are below 22% and 5% for the 1st- and 3rd-order approximations, with the maximum values at  $\alpha = \pi$ .

Combining Eqs. (6), (15) and (16), we can describe the torn geometry of the 2D sheet as

$$\sin\theta = \frac{f\gamma_i^2 l}{K\gamma_s t_s (1 - \cos\alpha)^2} + \frac{\sqrt{\gamma_i D} g(\alpha)}{\gamma_s t_s}$$

and the value averaged over the whole peeling process is

$$\langle \sin\theta \rangle = \frac{f\gamma_i^2}{K\gamma_s (1 - \cos\alpha)^2} \left( \frac{\langle l \rangle}{t_s} \right) + \frac{\sqrt{\gamma_i D}}{\gamma_s t_s} g(\alpha) \quad (19)$$

Here  $\langle l \rangle$  is the averaged value of  $l$  (Sen et al., 2010). Eqs. (14) and (19) are thus the solutions for the peeling force and the torn geometry, which will be used in the following discussion.

## 2.4. The peeling speed

In practice, the peeling kinetics plays an important role in the peeling process (Chen et al., 2013; Kovalchick et al., 2013). To elucidate the relationship between the peeling force  $F$  and speed  $v$ , for the sake of brevity, we consider a peeling-only process where the static peeling force  $F_0$  can be written as  $F_0 = \gamma_i w / (1 - \cos\alpha)$ . The dynamical nature of the peeling process introduces an additional kinetic peeling force  $F_1$ , which depends on the peeling speed  $v$ . According to the impulse-momentum theorem, we have  $F_1 dt = mv$ . Here  $F_1$  is the additional kinetic peeling force driving the speed of peeling front to change from 0 to  $v$  within  $dt$ ,  $m = \rho w dl$  is the effective mass of peeling front, where  $\rho$  is the areal mass density of peeling sheet, and  $w dl$  is the area. In addition,  $dl/dt = f_1 v$ , where  $f_1$  is a dimensionless factor characterizing the effect of peeling angle, we have  $F_1 = mdv/dt = \rho w v dl/dt = f_1 \rho w v^2$ , and thus

$$F = F_0 + F_1 = \frac{\gamma_i w}{1 - \cos\alpha} + f_1 \rho w v^2 \quad (20a)$$

Eq. (20a) can be re-written in the form of the 2D peeling stress defined as the peeling force per width, that is

$$\sigma_{2D} = \frac{F}{w} = \frac{\gamma_i}{1 - \cos\alpha} + f_1 \rho v^2 \quad (20b)$$

from which we find that  $\sigma_{2D}$  includes a static adhesion term  $\gamma_i / (1 - \cos\alpha)$ , and a kinetic, rate-dependent term  $f_1 \rho v^2$ .

## 2.5. Surface roughness of the substrate

The peeling force can also be modulated by the surface roughness of substrate (Zhao et al., 2013; Chen and Chen, 2013). We study this effect by considering a model substrate with continuously modulated profile  $h(x) = h_0 + A \sin(kx)$  with  $k = 2\pi/L$ . A characteristic factor of the roughness can be defined from the mean deviation of the profile from a flat surface, that is

$$R_s = \frac{A}{L} \propto \sqrt{\frac{\int_0^L h'(x)^2 dx}{L}} \quad (21)$$

To explore the effect of substrate roughness  $R_s$  on the peeling force, we consider the peeling process with an apparent peeling angle  $\beta = 90^\circ$  as shown in Fig. 3a, while the local peeling angle  $\alpha$  relative to the substrate depends on the surface morphology of the substrate. The 2D peeling stress  $\sigma_{2D} = \gamma_i / (1 - \cos\alpha)$  is a function of  $\alpha$ , and the peak value of 2D peeling stress  $\sigma_{2D}^P$  is reached at the maximum value of  $\cos\alpha$ , which plays an important role on the fracture of 2D sheets. Specifically, the slope of the profile is  $dh(x)/dx = Ak\cos(kx) = \tan(\beta - \alpha) = \cot(\alpha)$ , the maximum value is

$$\max(\cot\alpha) = Ak = 2\pi R_s$$

and the maximum value of  $\cos\alpha$  is

$$\max(\cos\alpha) = \frac{2\pi R_s}{\sqrt{(2\pi R_s)^2 + 1}}$$

Consequently, the peak value of the 2D peeling stress  $\sigma_{2D}^P$  is

$$\sigma_{2D}^P = \frac{\gamma_i}{[1 - \max(\cos\alpha)]} = \left[ (2\pi R_s)^2 + 2\pi R_s \sqrt{(2\pi R_s)^2 + 1} + 1 \right] \gamma_i \quad (22)$$

Eq. (22) thus demonstrates a quasi-quadratic dependence of  $\sigma_{2D}^P$  on  $R_s$ , and practically, the effect of surface roughness can be considered as a renormalized factor with additional interfacial adhesion.

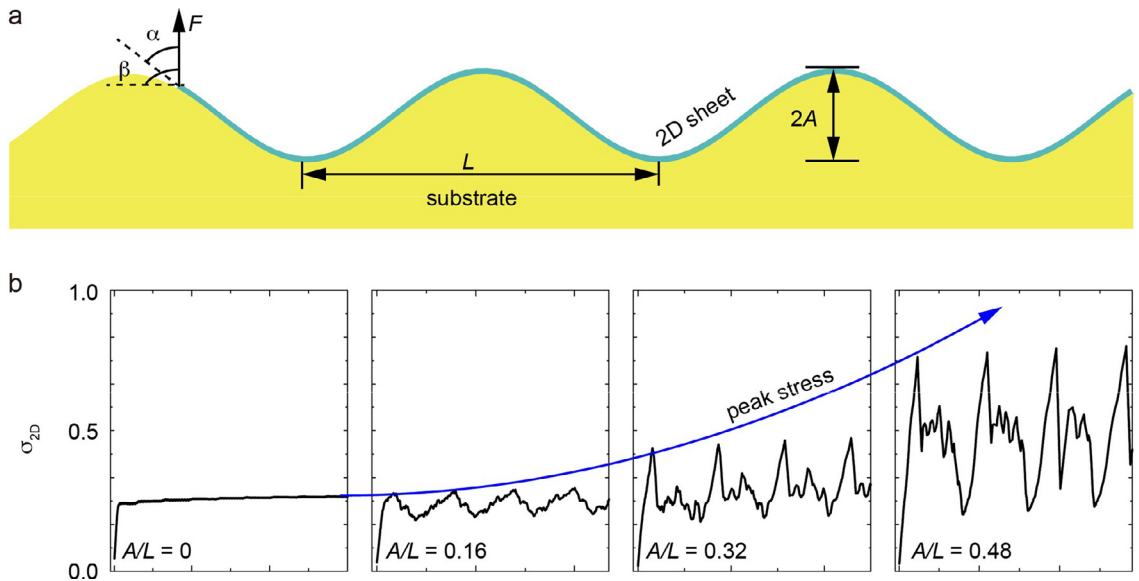


**Fig. 3.** (a) Schematic illustration of a 2D sheet peeled off from a rough substrate. (b) The CGMD simulation results show that the peak amplitudes of in-plane stress ( $\sigma_{2D}^2$ ) increases quadratically with the surface roughness, measured by the ratio  $A/L$ . Here the 2D stress is normalized by the tensile strength of the sheet.

### 3. Computer simulations

#### 3.1. First-principles calculations

The key parameters for the peeling process of 2D materials include the tensile stiffness  $K$ , the Poisson's ratio  $\nu$  for the in-plane elasticity, and bending stiffness  $D$  for out-of-plane deformation. To quantify these material parameters, we perform density functional theory (DFT) calculations using the Vienna *Ab-Initio Simulation Package* (VASP) (Kresse and Furthmüller, 1996). Plane-wave basis sets with an energy cut-off of 600 eV are used. The density of  $k$ -point mesh used in the reciprocal space is  $> 40 \text{ \AA}$ . The projected augmented wave (PAW) potentials are used for the ion-electron interactions, and the generalized gradient approximation (GGA) is used for the exchange-correlation functional in the Perdew-Burke-Ernzerhof (PBE) parametrization (Blochl, 1994; Perdew et al., 1997). Structural relaxation is performed for the primitive cells of all 2D materials using the conjugated-gradient algorithm. These settings are verified by an energy convergence threshold of 1 meV/atom, as well as thresholds for the force on each atom and the stress on each cell of 0.01 eV/ $\text{\AA}$  and 0.01 GPa, respectively.

To calculate the in-plane tensile properties, tensile tests are carried out on a rectangular supercell, by deforming the lattice in one direction while keeping the other lattice constant free to relax. Two methods were used to calculate the bending stiffness  $D$ . In the first one, a single-layer 2D sheet is rolled up into a cylindrical nanotube with a radius of  $R$ , and the value of  $D$  is extracted by fitting the strain energy density of the tubule  $E$ , i.e. the energy density difference between the tubule and the sheet, as a function of  $R$  following the relation  $E = D/(2R^2)$ . Depending on the direction of rolling process in the hexagonal lattice, the bending stiffness is calculated along the armchair and zigzag directions. Twenty special  $k$ -points sampled along the tube axis where the supercell is defined. In the fitting process, we use data for large-radius tubules to avoid the nonlinearity occurring at high curvature, which yields an accuracy in estimating  $D$  below 0.01 eV. In the second approach, we perform density functional perturbation theory (DFPT) based calculations using the VASP (Kresse and Furthmüller, 1996) and PHONOPY (Togo et al., 2008) packages. From the phonon dispersions  $\omega(q)$ , we calculate the group velocities of acoustic phonons, which are subsequently used to quantify mechanical properties of the 2D materials. Specifically, the flexural phonon mode ZA shows a quadratic dispersion (Karssemeijer and Fasolino, 2011), that is  $\omega^2 = (D/\rho)q^4$ . Here  $\rho$  is the areal density of mass. Fitting the dispersion  $\omega(q)$  with this equation above yields the value of  $D$ . We apply these two approaches to all 2D materials considered here except for MoS<sub>2</sub> and the silica bilayer, resulting in consistent values of  $D$ . Specifically, the difference in  $D$  values calculated for graphene is less than 0.1 eV. For MoS<sub>2</sub> and the silica bilayer, the tubule approach requires high computational costs and thus only DFPT calculations for  $D$  are performed.

#### 3.2. Coarse-grained model

Although the elastic deformation of 2D sheets can be described as a continuum without specific length scales, the advance of peeling and tearing fronts involves atomic-scale details. With the in-plane and out-of-plane mechanical properties

characterized by first-principles calculations (**Table S3**), we construct a coarse-grained model to simulate the mechanical exfoliation of 2D sheets on an adhesive substrate. In the coarse-grained molecular dynamics (CGMD) simulations, we consider potential energy contributions from the bond stretching, angle bending, and dihedrals terms, which are

$$V_b = k_b(d - d_0)^2 \quad (23a)$$

$$V_a = k_a(\theta - \theta_0)^2 \quad (23b)$$

$$V_d = k_d[1 - \cos(2\phi)] \quad (23c)$$

where  $d$ ,  $\theta$  and  $\phi$  are the bond length, angle, and dihedral angle, respectively. The parameters with subscript '0' are their values at equilibrium.  $k_b$ ,  $k_a$  and  $k_d$  are the spring constants for bonds, angles and dihedrals, which can be related to material parameters in the thin-shell model as

$$k_b = \frac{\sqrt{3}K}{2(1-\nu)} \quad (24a)$$

$$k_\theta = \frac{\sqrt{3}d_0^2 K}{12(1+3\nu)} \quad (24b)$$

and  $k_d$  can be fitted by bending tests from the value of  $D$ . The CG force field parameters for graphene used in this work are summarized in **Table S4**, and the model can be generalized for 2D materials with specific parameters fitted to our DFT calculation results. It should be noted that the harmonic description of Eq. (23a) cannot capture the nonlinear behavior and bond breaking events as the graphene sheet is torn. To solve this problem, we use a Morse-form potential function for the bond stretching energy, which captures the essential nonlinear behavior predicted by first-principles calculations (**Fig. S1**), that is

$$V_b = D_0[1 - e^{-A(d-d_0)}]^2 \quad (d < d_c) \quad (25)$$

where  $D_0$  and  $A$  are the depth and width of potential well, and  $d_c$  is the breaking bond length. In this force field, the anisotropy of edge energies (for armchair and zigzag) coincides with that predicted from the adaptive intermolecular reactive empirical bond-order (AIREBO) potential. This conclusion, however, conflicts with the result obtained from DFT calculations where the rearrangement of bond orders at the armchair edges is taken into account, which reduces the edge energy density to a value lower than that for the zigzag edge (**Fig. S2**) (Liu et al., 2010). The anisotropy in our CG model can be simply determined from the line density of  $sp^2$  bonds broken by cleaving cracks along the zigzag and armchair edges, which is  $3^{1/2}:2$ . Detailed parameters can be seen in **Table S4**. The interfacial adhesion is modeled by the 12-6 Lennard-Jones (L-J) potential

$$V_{LJ} = 4\varepsilon \left[ \left( \frac{\sigma}{r} \right)^{12} - \left( \frac{\sigma}{r} \right)^6 \right] \quad (26)$$

where  $\varepsilon$  is the depth of the L-J potential well between the CG bead in 2D sheets and the substrate, and  $\sigma$  is the L-J parameter associated with the equilibrium distance ( $2^{1/6}\sigma$ ). These parameters are obtained by fitting interfacial properties (**Fig. S3**). This approach has been successfully applied to model the elastic responses of graphene sheets (Ruiz et al., 2015), and their interfaces with substrates (Qin et al., 2015).

In the CGMD simulations of tearing, a 2D sheet is deposited on to a rigid surface (**Fig. 1d**). Two notches are created on the edges and a rectangular flap is pulled upwards at a constant speed  $v$  and angle  $\alpha$ . The two crack tips at the flap edges are set in parallel initially, which subsequently propagate forwards or inwards as the sheet detaches from the substrate. A strip is eventually separated from the mother sheet completely, leaving behind a triangular tearing of 2D sheet. **Fig. 1d** illustrates the peeling processes for different interfacial adhesive strengths. Specifically, for the peeling of graphene, we model a  $6 \times 6 \mu\text{m}$  sheet represented by 17,200 CG beads, as summarized in **Table S4**, and carried out a set of numerical simulations to explore the interplay between deformation and geometry in the forced peeling process of 2D materials.

#### 4. Simulation results and discussions

In this section, we present our CGMD simulation results for the peeling and tearing processes of 2D materials adhered to the substrate, to probe the roles of controlling parameters. The results are discussed based on the theory we developed in **Section 2**. We will focus on the key factors (the peeling angle, speed, and substrate roughness) that influence the amplitude of peeling force  $F$  and the feasibility of mechanical exfoliation for specific sheet-substrate pairs first, and then explore the geometrical development of the torn sheets, and the way to control the dynamical process and the torn patterns.

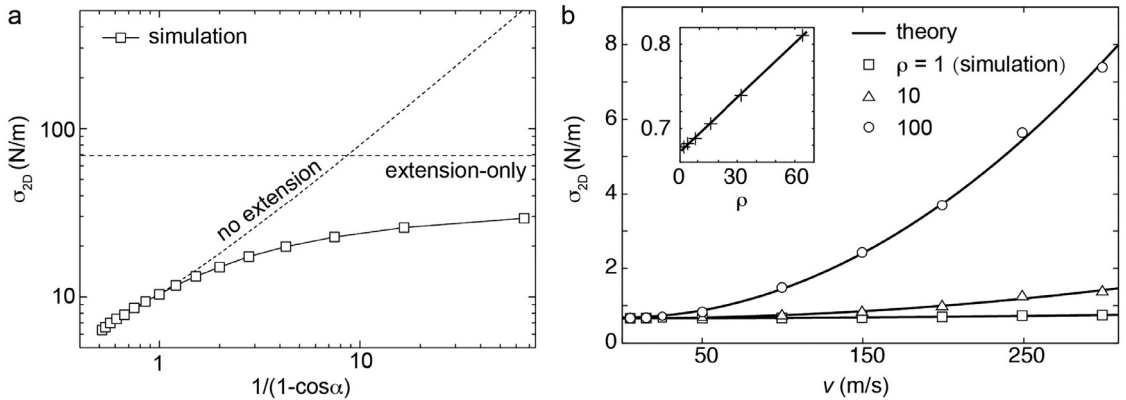


**Fig. 4.** (a) The 2D stress  $\sigma_{2D}$  obtained from CGMD simulations aligns with theoretical predictions with the no-extension approximation as the factor  $(1 - \cos\alpha)^{-1}$  is small and approaches the extension-only extreme as the factor increases. (b)  $\sigma_{2D}$  in sheets obtained by CGMD simulations shows a quadratic dependence on the peeling speed  $v$  and a linear dependence on the areal mass density  $\rho$  of the 2D sheet normalized by that of graphene.

#### 4.1. Peeling force

From Eq. (14), we find that the essential physics of the peeling and tearing process can be captured by inspecting the edge cleavage term  $2\gamma_{st}s\cos\theta$  and the nonlinear term  $(1-f)F^2/Kw$ , in addition to the contribution from interfacial adhesion term  $\gamma_i w$ . For a typical sheet of 2D materials with lateral size of  $1\text{--}10\mu\text{m}$ , the value of  $\gamma_{st}s$  is 2–4 orders lower than that of typical values of  $\gamma_i w$ , and the edge cleavage term takes effect on the peeling force only as the width is reduced below a critical value  $\sim\gamma_{st}s/\gamma_i$  (on the order of 10 nm for graphene) with the notches propagating forward and inward. To assess the role of the nonlinear term in Eq. (14), a set of peeling simulations are conducted at different peeling angles. The results in Fig. 4a clearly show that this nonlinear term is activated as  $\alpha$  approaches  $0^\circ$ , where the dash lines indicate the limits without extension or with extension only, which was previously discussed in macroscopic peeling experiments (Kendall, 1975), where the force required to peel an elastic film off from a rigid substrate depends not only on the adhesive surface energy but also on an elastic deformation term. The nonlinear term in Eq. (14), which reduces the peeling force, becomes significant only in two specific instances – the material could sustain 2D stress  $\sigma_{2D}=F/w$  up to  $K/10$  before breakage, or at very low peeling angles.

As the kinetic effect is taken into account, we expect a distinct velocity-dependence of  $F$  from Eq. (20). CGMD simulations at various peeling speeds and areal mass densities are performed for typical 2D materials at a constant peeling angle of  $90^\circ$ . The results are in consistency with our theoretical predictions (Eq. (20)), revealing that  $F$  has a linear and quadratic dependence on areal mass density  $\rho$  and peeling velocity  $v$ , respectively (Fig. 4b). The effect of the peeling velocity on  $F$ , as a measure of the kinetic effect, becomes apparent only as  $v$  exceeds  $\sim 10\text{ m/s}$ , which is quite high compared to that in the macroscopic peeling tests where the kinetic effect is significant even at  $v=\sim 10\mu\text{m/s}$  (Kovalchick et al., 2013). This discrepancy across the length scales originates from the competition between the rate-dependence of peeling and the static adhesion that determine the peeling force in Eq. (20a), where the value of  $F$  is less sensitive to the peeling velocity for 2D sheets due to the low areal mass density.

For rough surfaces, the 2D peeling stress  $\sigma_{2D}=\gamma_i/(1-\cos\alpha)$  is not a constant as the peeling angle  $\alpha$  depends on the local morphology of the substrate, and is maximized at the highest value of  $\cos\alpha$ . Considering that the peak value of 2D peeling stress  $\sigma_{2D}^P$  controls the fracture of 2D sheets in the peeling process, the discussion is focused on  $\sigma_{2D}^P$ . Eq. (21) predicts the correlation between the peak value of  $F$  and the surface roughness  $R_s$ . It indicates that the peak amplitude of  $F$  increases as a quasi-quadratic function of  $R_s$ , which matches our CGMD simulation results in Fig. 3b.

We now assess the feasibility of mechanical exfoliation or transfer for a specific 2D sheet-substrate pair. During the peeling process, the 2D stress in the sheet adhered to a flat substrate can be explicitly expressed as  $\sigma_{2D}=\frac{\gamma_i}{1-\cos\alpha}$  if the nonlinear force and edge cleavage terms in Eq. (14) as well as the kinetic effects in Eq. (20b) are neglected, which arise only in extreme situations as we discussed, and if the surface roughness is further considered, the peak stress is  $\sigma_{2D}^P=[(2\pi R_s)^2+2\pi R_s\sqrt{(2\pi R_s)^2+1}+1]\gamma_i$  (Eq. (22)). Consequently, for a specific peeling setup, we can define a criterion

$$\frac{\sigma_s}{\gamma_i} > C = \frac{\sigma_{2D}}{\gamma_i} = \begin{cases} \frac{1}{1-\cos\alpha} & \text{for flat surfaces} \\ \frac{[(2\pi R_s)^2+2\pi R_s\sqrt{(2\pi R_s)^2+1}+1]\gamma_i}{\gamma_i} & \text{for rough surfaces} \end{cases} \quad (27)$$

2D sheet-substrate pairs with dimensionless factors of peeling feasibility  $\frac{\sigma_s}{\gamma_i}$  above  $C$  can be exfoliated or peeled off without break the material integrity in the specific peeling setup. Based on our first-principles calculation results and data collected from literature, the dimensionless parameter  $\sigma_s/\gamma_i$  for typical pairs of 2D materials and substrates are evaluated

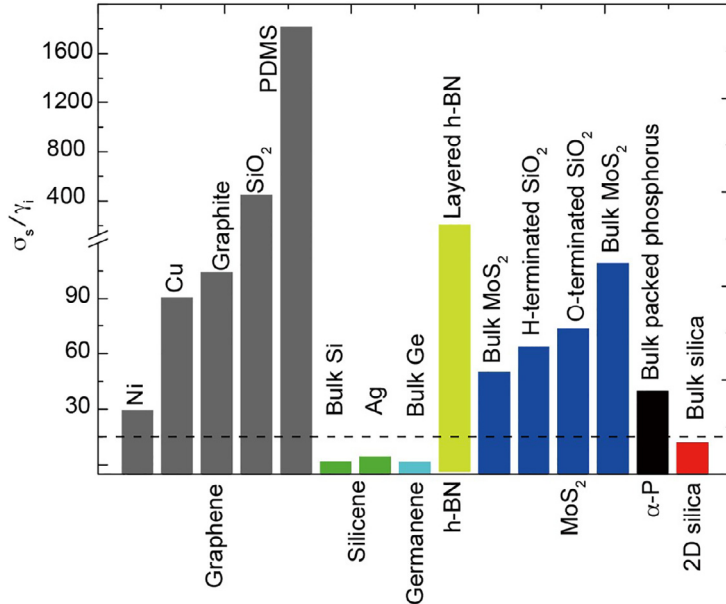


**Fig. 5.** The feasibility factor  $\sigma_s/\gamma_i$  calculated for 2D sheets on the substrate. The dash line with value  $C = 15$  defines the criterion above which successful exfoliation was experimentally achieved, as reported in the references listed in the Supplementary Material (Table S1).

and summarized in Fig. 5. By noting that 2D materials such as graphene, MoS<sub>2</sub>, h-BN and black phosphorus can be exfoliated as suspended monolayers from layered assemblies or selected substrates (Castellanos-Gomez et al., 2014; Geim and Novoselov, 2007; Gorbatchev et al., 2011; Li et al., 2014), while monolayer silicene and germanene have not yet been exfoliated successfully yet, we conclude that value of  $C$  is about 15, which is accessible in typical peeling setups according to the definition in Eq. (27). For comparison, the value of  $\sigma_s/\gamma_i$  is  $\sim 9\text{--}24$  for macroscopic scotch-tape tests (Table S2 and Fig. S4), where the tape adhered to typical surfaces can be successfully peeled off with a peeling angle except for those with extremely values of  $\alpha$  (Coleman et al., 2011).

#### 4.2. Torn geometry

Tearing a sheet from a substrate is the key process for mechanical exfoliation and transfer. The torn part of materials not only determines the area of 2D sheets that can be obtained, but also can be tuned to produce samples with specific geometries that could be important for specific optical-electronic applications (Sen et al., 2010). With the definition of bending and tensile stiffness  $D = Yt_s^3/[12(1 - \nu^2)]$  and tensile stiffness  $K = Yt_s$ , one can rewrite the value of  $\sin\theta$  in Eq. (19) averaged over the peeling process as  $\langle \sin\theta \rangle = f\gamma_i^2 \langle l \rangle / [Y\gamma_s t_s^2 (1 - \cos\alpha)^2] + (\gamma_i Yt_s / [12(1 - \nu^2)])^{1/2} g(\alpha) / \gamma_s$ , where  $\langle l \rangle$  is the averaged value of  $l$ . Then the control of torn geometry of 2D sheets can be discussed in two regimes. Firstly, as the stretching term dominates, we have

$$\langle \sin\theta_s \rangle = \frac{f\gamma_i^2}{Yt_s \gamma_s (1 - \cos\alpha)^2} \left( \frac{\langle l \rangle}{t_s} \right) \quad (28a)$$

while as the bending term dominates,

$$\langle \sin\theta_b \rangle = \sqrt{\frac{Yt_s \gamma_i}{12(1 - \nu^2) \gamma_s^2}} g(\alpha) \quad (28b)$$

It can be seen clearly from Eqs. (28a) and (28b) that the tearing angle decreases with  $t_s$  if stretching-dominates, while increases with  $t_s$  in the bending-dominated regime. For example, with a typical set of parameters  $\gamma_s t_s = 2.2 \text{ eV}/\text{\AA}$ ,  $\gamma_i = 0.5 \text{ J/m}^2$ ,  $K = 345 \text{ N/m}$ ,  $f = 0.5$ ,  $\langle l \rangle = 2 \mu\text{m}$  for graphene (Sen et al., 2010), the values of  $\sin\theta_s$  and  $\sin\theta_b$  can be plotted as a function of  $t_s$  (Fig. 6). There is a distinct transition from the stretching- to bending-dominated regimes as indicated by the value of  $\sin\theta$ , and the critical value of  $t_s$  is 0.336 nm. For a monolayer graphene, the thin-shell thickness is 0.089 nm  $< 0.336 \text{ nm}$  (Gao and Xu, 2015), and thus the torn geometry is controlled by the stretching term, as shown in Fig. 6. In addition, from Eqs. (28a) and (28b), we find that if the stretching term dominates, the tearing angle  $\theta$  decreases with the peeling angle  $\alpha$ . While if the bending term dominates, the trend is reversed. In our CGMD simulations for graphene peeled at angle  $\alpha = 30^\circ\text{--}150^\circ$ , the value of  $\theta$  decreases with  $\alpha$  as the sheet is peeled from either the zigzag or armchair directions (Fig. 7).

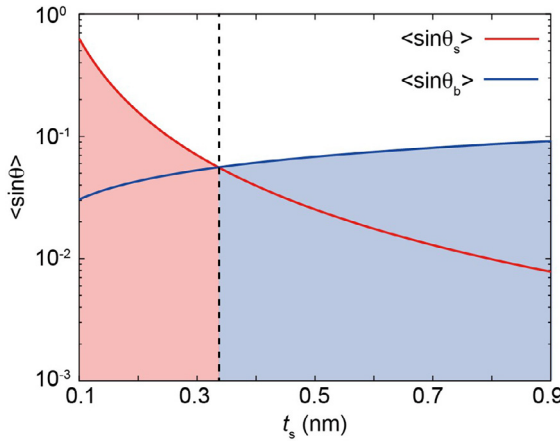


**Fig. 6.** The torn geometry of 2D sheets measured in  $\langle \sin\theta \rangle$ , which is controlled by stretching for sheets with small values of  $t_s$  ( $\sin\theta_s$ ), and bending for those with large values of  $t_s$  ( $\sin\theta_b$ ).

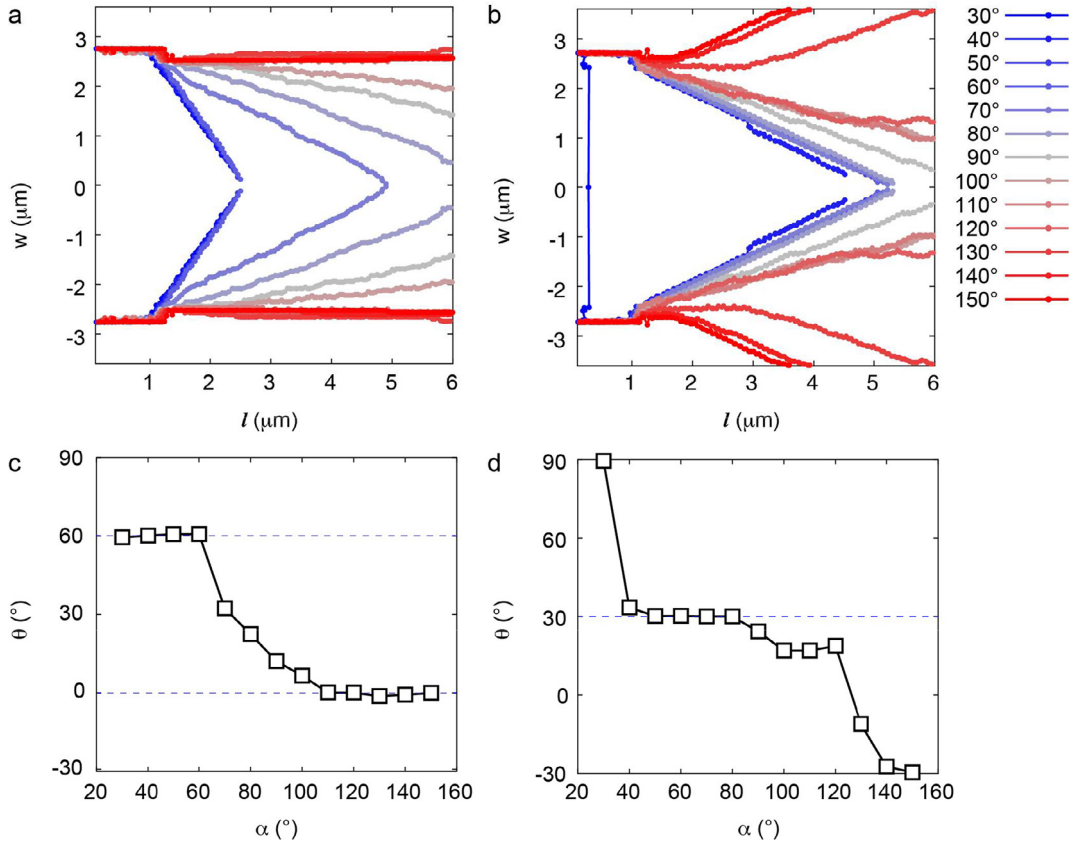


**Fig. 7.** (a, b) Geometrical evolution of 2D sheets torn at different peeling angles  $\alpha$  from  $30^\circ$  to  $150^\circ$ . (c, d) The tearing angle  $\theta$  decreases with  $\alpha$ . The development of crack prefers to proceed along the zigzag direction, as the fracture at peeling front is controlled by the local strength of atomic bonds (Yin et al., 2015). The peeling direction is aligned to the zigzag and armchair directions for panels a,c and b,d, respectively.

which verifies the fact that the shape of torn pattern is determined by the stretching term. In contrast, in macro-scale tearing experiments, the torn shape is controlled by the bending term considering the much larger sheet thickness, resulting in totally different tearing behaviors (Kruglova et al., 2011).

We also conclude from the CGMD simulations that crack advancing along the zigzag direction is preferred in the process. These results may be related to the orientation dependence of the edge energy, which is the lowest for the zigzag edge while the highest for the armchair edge, as predicted by the potential used in our CGMD simulations as well as full-atom MD simulations using the AIREBO potential. This result is contrary to that obtained from DFT and reactive force field

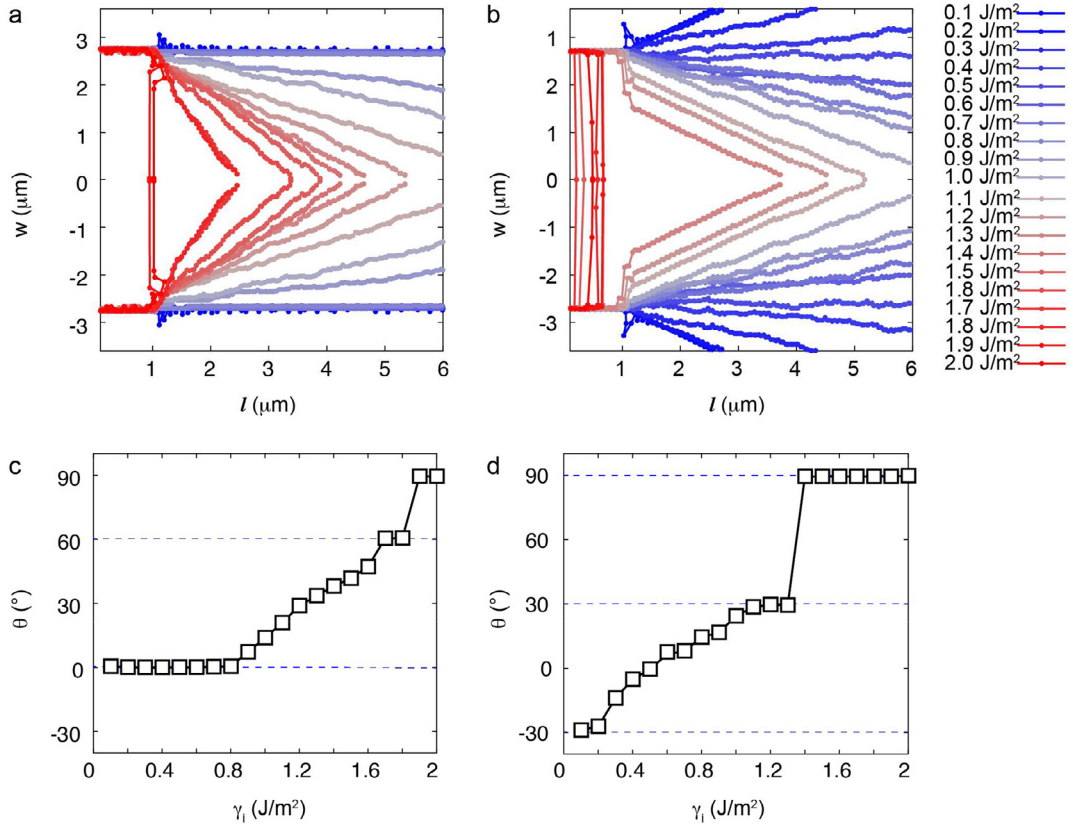


**Fig. 8.** (a, b) Geometrical evolution of torn 2D sheets at different interfacial adhesive strength  $\gamma_i$  from 0.1 to 2.0 J/m<sup>2</sup>. (c, d) The tearing angle  $\theta$  increases with  $\gamma_i$ , and the development of crack prefers to proceed along the zigzag direction. The peeling direction is aligned to the zigzag and armchair directions for panels a, c and b, d, respectively.

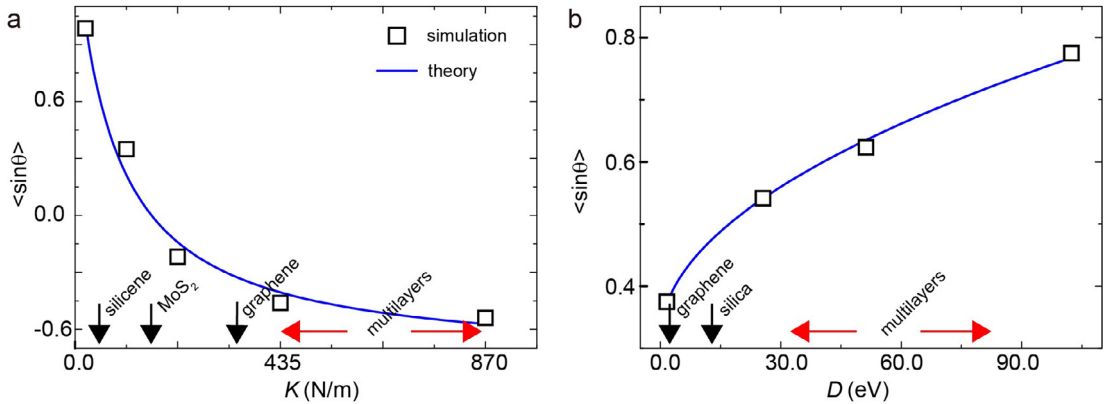


**Fig. 9.** The relation between the torn geometry, defined through the value of  $\sin\theta$  averaged over the peeling process,  $\langle \sin\theta \rangle$ , decreases with the tensile stiffness  $K$ , while increases with the bending stiffness  $D$  of the 2D sheets, as demonstrated by the CGMD simulation results that align well with theoretical predictions from Eq. (19). By increasing the value of  $K$ , the torn sheet becomes wider as the peeling process proceeds, while as  $D$  increases, the torn sheet becomes narrower.

(ReaxFF) calculations where the environment dependence of bond orders is considered (Fig. S2). On the other hand, Yin et al. show that crack extension in graphene prefers to proceed along the zigzag edge, based on their AIREBO and DFT calculations, and conclude that the determination of crack advancing direction is controlled by the local strength-based failure criterion (Yin et al., 2015) rather than the edge-energy-based criterion (Kim et al., 2011), where the fracture of lattice is determined by the elongation of  $sp^2$  bonds locally (Xu, 2009). Both armchair and zigzag edges were characterized in graphene cut mechanically (Mohanty et al., 2012). Yang et al. found that there is a specific preference of the direction of the cleaved edges in the exfoliated samples of graphene. However, the armchair and zigzag nature of graphene edges was not directly

characterized in this study, leaving the determination of brittle fracture mechanisms an open issue, from the experimental perspective (Yang et al., 2017). It should also be noted that, although our theoretical predictions here, in general, agree with the CGMD simulation result, the anisotropic nature of the edge energy density for graphene has not been considered in our continuum mechanics theory (Fig. S2), which may further validate the local-strength argument for the failure criterion. In presence of defects, the peeling and tearing processes can be modified. Firstly, material and interfacial properties will be revised, which can be discussed based on our model. Secondly, the defects may deviate the pathway of crack propagation in the 2D materials and thus change the morphology of torn sheets. In the continuum model, the effects of detailed atomic structures can be taken into account for through the parameters, which could influence the peeling force and tearing morphology. We believe that the multilayered or buckled structures of 2D materials other than graphene and h-BN will result in richer fracture behaviors that remain to be explored in future studies. Moreover, for anisotropic materials such as phosphorene (Sorkin and Zhang, 2015), the chirality-dependent elastic responses and edge cleavage energies have to be included according to the orientation of lattice as well as the peeling setup, which will modify the peeling and tearing processes according to Eq. (27), where the feasibility can be assessed.

In addition to the peeling angle, the adhesive strength between 2D sheets and the substrate is another key factor for mechanical exfoliation. To explore the effect of substrate adhesion on the tearing angle  $\theta$ , we performed CGMD simulations with  $\gamma_i = 0.1\text{--}2.0 \text{ J/m}^2$ . The results indicate that no matter when graphene is peeled along the zigzag or the armchair directions, the value of  $\theta$  increases with  $\gamma_i$  (Fig. 8), and the crack advancing prefers to be along zigzag edges following the local-strength criterion of fracture. Additional CGMD simulations at angle  $\alpha = 90^\circ$  are conducted to probe the effects of tensile and bending stiffness for various 2D materials. These results show that the area of the torn sheet increases with  $K$ , but decreases with  $D$  (Fig. 9), in consistency with the predictions from Eqs. (28a) and (28b). These results indicate that the torn geometry of 2D sheets from mechanical exfoliation could be finely tuned through the interfacial and material properties.

## 5. Conclusions

In this work, we have presented both theoretical analysis and computational simulation results to explore the peeling and tearing behaviors of 2D materials from a solid substrate, which is of critical importance to control the process of mechanical exfoliation or transfer. We propose a criterion to measure the feasibility of peeling off 2D sheets from the adhesive substrates, by comparing the dimensionless factor  $\sigma_s/\gamma_i$  with a parameter  $C$  that is determined by the peeling setup. The material properties, geometrical and kinetic factors in the peeling setup that modulate the peeling behaviors of sheets and their torn morphology are discussed, offering guidelines to optimize the process for high efficiency and yield. We validated our theoretical models by comparing the model predictions and CGMD simulation results. We find that from practical consideration, one could conclude from the results presented here that the peeling angle and adhesive strength are the most effective factors to control the peeling process, and could be feasibly tuned in experiments. The theoretical model and simulation tools proposed here could help optimize the exfoliation or transfer processes. In addition, recently high-throughput computation and data mining were applied to assess the exfoliation feasibility of 2D materials through the atomic structures and interlayer binding energy of their bulk compounds (Lebegue et al., 2013; Mounet et al., 2018), which could be further improved by incorporating the key parameters identified in our conclusion.

## Acknowledgments

This work was supported by MIT Seed Funds: Greater China Fund of Innovation. E.G., S.-Z.L., X.-Q.F. and Z.X. were supported by the National Natural Science Foundation of China through Grants 11222217 and 11432008, the State Key Laboratory of Mechanics and Control of Mechanical Structures (Nanjing University of Aeronautics and Astronautics) through Grant no. MCMS-0414G01, and the Opening Project of Applied Mechanics and Structure Safety Key Laboratory of Sichuan Province through Grant SZDKF-1601. Z.Q. and M.J.B acknowledge support from the Office of Naval Research (Grant no. N00014-16-1-2333). The computation was performed on the Explorer 100 cluster system of Tsinghua National Laboratory for Information Science and Technology.

## Appendix

**Appendix Table 1.**

**Appendix 1**  
List of key variables used in the text.

Symbols	Variables
$F$	Peeling force
$\sigma_{2D}$	2D peeling stress
$\sigma_s$	2D strength of 2D sheets
$\alpha$	Peeling angle
$v$	Peeling speed
$\theta$	Tearing angle
$w_0$	Initial width of the peeled sheet
$w$	The width of the peeling front
$\gamma_i$	The adhesive energy per unit area of interface
$\gamma_s$	Work of fracture per unit area of the 2D sheet
$t_s$	Thickness of the 2D sheet
$s$	Crack length
$l$	The distance that the peeling front travels
$\langle l \rangle$	The value of $l$ averaged over the peeling process
$U$	Total energy of the 2D sheet-substrate system
$U_T$	Stretching energy of the 2D sheet
$U_B$	Bending energy of the 2D sheet
$U_E$	Elastic deformation energy of the 2D sheet
$D$	Bending stiffness of the 2D sheet
$K$	Tensile stiffness of the 2D sheet
$\nu$	In-plane Poisson's ratio of the 2D sheet
$R_s$	Surface roughness of the substrate

## Supplementary materials

Supplementary material associated with this article can be found, in the online version, at doi:[10.1016/j.jmps.2018.03.014](https://doi.org/10.1016/j.jmps.2018.03.014).

## References

- Allen, M.J., Tung, V.C., Gomez, L., Xu, Z., Chen, L.M., Nelson, K.S., Zhou, C.W., Kaner, R.B., Yang, Y., 2009. Soft transfer printing of chemically converted graphene. *Adv. Mater.* 21, 2098–2102.
- Allen, M.J., Tung, V.C., Kaner, R.B., 2010. Honeycomb carbon: a review of graphene. *Chem. Rev.* 110, 132–145.
- Blees, M.K., Barnard, A.W., Rose, P.A., Roberts, S.P., McGill, K.L., Huang, P.Y., Ruyack, A.R., Kevek, J.W., Kobrin, B., Muller, D.A., McEuen, P.L., 2015. Graphene kirigami. *Nature* 524, 204–207.
- Blochl, P.E., 1994. Projector augmented-wave method. *Phys. Rev. B* 50, 17953–17979.
- Butler, S.Z., Hollen, S.M., Cao, L., Cui, Y., Gupta, J.A., Gutierrez, H.R., Heinz, T.F., Hong, S.S., Huang, J., Ismach, A.F., Johnston-Halperin, E., Kuno, M., Plashnitsa, V.V., Robinson, R.D., Ruoff, R.S., Salahuddin, S., Shan, J., Shi, L., Spencer, M.G., Terrones, M., Windl, W., Goldberger, J.E., 2013. Progress, challenges, and opportunities in two-dimensional materials beyond graphene. *ACS Nano* 7, 2898–2926.
- Castellanos-Gomez, A., Vicarelli, L., Prada, E., Island, J.O., Narasimha-Acharya, K.L., Blanter, S.I., Groenendijk, D.J., Buscema, M., Steele, G.A., Alvarez, J.V., Zandbergen, H.W., Palacios, J.J., van der Zant, H.S.J., 2014. Isolation and characterization of few-layer black phosphorus. *2D Mater.* 1, 025001.
- Chen, H., Feng, X., Huang, Y., Huang, Y.G., Rogers, J.A., 2013. Experiments and viscoelastic analysis of peel test with patterned strips for applications to transfer printing. *J. Mech. Phys. Solids* 61, 1737–1752.
- Chen, H., Chen, S., 2013. The peeling behaviour of a graphene sheet on a nano-scale corrugated surface. *J. Phys. D* 46, 435305.
- Coleman, J.N., Lotya, M., O'Neill, A., Bergin, S.D., King, P.J., Khan, U., Young, K., Gaucher, A., De, S., Smith, R.J., Shvets, I.V., Arora, S.K., Stanton, G., Kim, H.Y., Lee, K., Kim, G.T., Duesberg, G.S., Hallam, T., Boland, J.J., Wang, J.J., Donegan, J.F., Grunlan, J.C., Moriarty, G., Shmeliov, A., Nicholls, R.J., Perkins, J.M., Grieveson, E.M., Theuwissen, K., McComb, D.W., Nellist, P.D., Nicolosi, V., 2011. Two-dimensional nanosheets produced by liquid exfoliation of layered materials. *Science* 331, 568–571.
- Gao, E., Xu, Z., 2015. Thin-shell thickness of two-dimensional materials. *J. Appl. Mech.* 82, 121012.
- Geim, A.K., Grigorieva, I.V., 2013. Van der waals heterostructures. *Nature* 499, 419–425.
- Geim, A.K., Novoselov, K.S., 2007. The rise of graphene. *Nat. Mater.* 6, 183–191.
- Gorbachev, R.V., Riaz, I., Nair, R.R., Jalil, R., Britnell, L., Belle, B.D., Hill, E.W., Novoselov, K.S., Watanabe, K., Taniguchi, T., Geim, A.K., Blake, P., 2011. Hunting for monolayer boron nitride: optical and Raman signatures. *Small* 7, 465–468.
- Hamm, E., Reis, P., LeBlanc, M., Roman, B., Cerdá, E., 2008. Tearing as a test for mechanical characterization of thin adhesive films. *Nat. Mater.* 7, 386–390.
- Huang, Y., Wu, J., Hwang, K.C., 2006. Thickness of graphene and single-wall carbon nanotubes. *Phys. Rev. B* 74, 245413.
- Karssemeijer, L.J., Fasolino, A., 2011. Phonons of graphene and graphitic materials derived from the empirical potential LCBOPII. *Surf. Sci.* 605, 1611–1615.
- Kendall, K., 1975. Thin-film peeling-the elastic term. *J. Phys. D* 8, 1449–1452.
- Kim, H., Jung, M.W., Myung, S., Jung, D., Lee, S.S., Kong, K.J., Lim, J., Lee, J.H., Park, C.Y., An, K.S., 2013. Soft lithography of graphene sheets via surface energy modification. *J. Mater. Chem. C* 1, 1076–1079.
- Kim, K., Artyukhov, V.I., Regan, W., Liu, Y., Crommie, M.F., Yakobson, B.I., Zettl, A., 2011. Ripping graphene: preferred directions. *Nano Lett.* 12, 293–297.
- Kim, K.S., Aravas, N., 1988. Elastoplastic analysis of the peel test. *Int. J. Solids Struct.* 24, 417–435.
- Koskinen, P., Kit, O.O., 2010. Approximate modeling of spherical membranes. *Phys. Rev. B* 82, 235420.
- Kotov, N.A., Weiss, P.S., 2014. Self-assembly of nanoparticles: a snapshot. *ACS Nano* 8, 3101–3103.
- Kovalchick, C., Molinari, A., Ravichandran, G., 2013. Rate dependent adhesion energy and nonsteady peeling of inextensible tapes. *J. Appl. Mech.* 81, 041016.
- Kresse, G., Furthmüller, J., 1996. Efficient iterative schemes for *ab initio* total-energy calculations using a plane-wave basis set. *Phys. Rev. B* 54, 11169–11186.
- Kruglova, O., Brau, F., Villers, D., Damman, P., 2011. How geometry controls the tearing of adhesive thin films on curved surfaces. *Phys. Rev. Lett.* 107.
- Kudin, K.N., Scuseria, G.E., Yakobson, B.I., 2001.  $C_2F BN$ , and  $C$  nanoshell elasticity from *ab initio* computations. *Phys. Rev. B* 64, 235406.
- Lebegue, S., Björkman, T., Klintenberg, M., Nieminen, R.M., Eriksson, O., 2013. Two-dimensional materials from data filtering and *ab initio* calculations. *Phys. Rev. X* 3, 031002.
- Li, H., Wu, J., Yin, Z., Zhang, H., 2014. Preparation and applications of mechanically exfoliated single-layer and multilayer MoS<sub>2</sub> and WSe<sub>2</sub> nanosheets. *Acc. Chem. Res.* 47, 1067–1075.

- Li, T.S., 2012. Ideal strength and phonon instability in single-layer MoS<sub>2</sub>. *Phys. Rev. B* 85, 235407.
- Liu, F., Ming, P., Li, J., 2007. *Ab initio* calculation of ideal strength and phonon instability of graphene under tension. *Phys. Rev. B* 76, 064120.
- Liu, Y., Dobrinsky, A., Yakobson, B.I., 2010. Graphene edge from armchair to zigzag: the origins of nanotube chirality? *Phys. Rev. Lett.* 105, 235502.
- Novoselov, K.S., Geim, A.K., Morozov, S.V., Jiang, D., Katsnelson, M.I., Grigorieva, I.V., Dubonos, S.V., Firsov, A.A., 2005. Two-dimensional gas of massless dirac fermions in graphene. *Nature* 438, 197–200.
- Mohanty, N., Moore, D., Xu, Z., Sreeprasad, T.S., Nagaraja, A., Rodriguez, A.A., Berry, V., 2012. Nanotomy-based production of transferable and dispersible graphene nanostructures of controlled shape and size. *Nat. Commun.* 3, 844.
- Mounet, N., Gibertini, M., Schwaller, P., Campi, D., Merkys, A., Marrazzo, A., Sohier, T., Castelli, I.E., Cepellotti, A., Pizzi, G., Marzari, N., 2018. Two-dimensional materials from high-throughput computational exfoliation of experimentally known compounds. *Nat. Nanotechnol.* 13, 246–252.
- Novoselov, K.S., Geim, A.K., Morozov, S.V., Jiang, D., Zhang, Y., Dubonos, S.V., Grigorieva, I.V., Firsov, A.A., 2004. Electric field effect in atomically thin carbon films. *Science* 306, 666–669.
- Perdew, J.P., Burke, K., Ernzerhof, M., 1997. Generalized gradient approximation made simple. *Phys. Rev. Lett.* 78, 1396.
- Peng, Z., Chen, S., 2015. Effect of bending stiffness on the peeling behavior of an elastic thin film on a rigid substrate. *Phys. Rev. E* 91, 042401.
- Pumera, M., Ambrosi, A., Bonanni, A., Chng, E.L.K., Poh, H.L., 2010. Graphene for electrochemical sensing and biosensing. *Trends Anal. Chem.* 29, 954–965.
- Qin, Z., Xu, Z., Buehler, M.J., 2015. Peeling silicene from model silver substrates in molecular dynamics simulations. *J. Appl. Mech.* 82, 101003.
- Rivlin, R.S., 1944. The effective work of adhesion. *Paint Technol.* 9, 215–218.
- Ruiz, L., Xia, W.J., Meng, Z.X., Keten, S., 2015. A coarse-grained model for the mechanical behavior of multi-layer graphene. *Carbon* 82, 103–115.
- Sen, D., Novoselov, K.S., Reis, P.M., Buehler, M.J., 2010. Tearing graphene sheets from adhesive substrates produces tapered nanoribbons. *Small* 6, 1108–1116.
- Shao, Y.Y., Wang, J., Wu, H., Liu, J., Aksay, I.A., Lin, Y.H., 2010. Graphene based electrochemical sensors and biosensors: a review. *Electroanalysis* 22, 1027–1036.
- Sorkin, V., Zhang, Y.W., 2015. The deformation and failure behaviour of phosphorene nanoribbons under uniaxial tensile strain. *2D Mater.* 2, 035007.
- Togo, A., Oba, F., Tanaka, I., 2008. First-principles calculations of the ferroelastic transition between rutile-type and CaCl<sub>2</sub>-type SiO<sub>2</sub> at high pressures. *Phys. Rev. B* 78, 134106.
- Tvergaard, V., Hutchinson, J.W., 1992. The relation between crack-growth resistance and fracture process parameters in elastic plastic solids. *J. Mech. Phys. Solids* 40, 1377–1397.
- Varoon, K., Zhang, X., Elyassi, B., Brewer, D.D., Gettel, M., Kumar, S., Lee, J.A., Maheshwari, S., Mittal, A., Sung, C.Y., Cococcioni, M., Francis, L.F., McCormick, A.V., Mkhitaryan, K.A., Tsapatsis, M., 2011. Dispersible exfoliated zeolite nanosheets and their application as a selective membrane. *Science* 334, 72–75.
- Wei, N., Peng, X., Xu, Z., 2014. Breakdown of fast water transport in graphene oxides. *Phys. Rev. E* 89, 012113.
- Wei, Y., Hutchinson, J.W., 1998. Interface strength, work of adhesion and plasticity in the peel test. *Int. J. Fract.* 93, 315–333.
- Xu, Z., 2009. Graphene nanoribbon under tension. *J. Comput. Theor. Nanosci.* 6, 625–628.
- Xu, Z., 2016. Defects in two-dimensional materials: topological and geometrical effects. *Chin. Sci. Bull.* 61, 501–510.
- Yang, J., Wang, Y., Li, Y., Gao, H., Chai, Y., Yao, H., 2017. Edge orientations of mechanically exfoliated anisotropic two-dimensional materials. *J. Mech. Phys. Solids* 112, 157–168.
- Yi, M., Shen, Z.G., 2015. A review on mechanical exfoliation for the scalable production of graphene. *J. Mater. Chem. A* 3, 11700–11715.
- Yin, H., Qi, H.J., Fan, F., Zhu, T., Wang, B., Wei, Y., 2015. Griffith criterion for brittle fracture in graphene. *Nano Lett.* 15, 1918–1924.
- Zhang, D.B., Akatyeva, E., Dumitrica, T., 2011. Bending ultrathin graphene at the margins of continuum mechanics. *Phys. Rev. Lett.* 106, 255503.
- Zhao, H.P., Wang, Y.C., Li, B.W., Feng, X.Q., 2013. Improvement of the peeling strength of thin films by a bioinspired hierarchical interface. *Int. J. Appl. Mech.* 15, 1350012.

# **Supplementary Material for**

## **Mechanical Exfoliation of Two-Dimensional Materials**

Enlai Gao<sup>1</sup>, Shao-Zhen Lin<sup>1,2</sup>, Zhao Qin<sup>3,4</sup>, Markus J. Buehler<sup>3,4</sup>, Xi-Qiao Feng<sup>1,2</sup>,  
Zhiping Xu<sup>1,5,\*</sup>

<sup>1</sup>Applied Mechanics Laboratory, Department of Engineering Mechanics and Center  
for Nano and Micro Mechanics, Tsinghua University, Beijing 100084, China.

<sup>2</sup>Institute of Biomechanics and Medical Engineering, Tsinghua University, Beijing  
100084, China

<sup>3</sup>Laboratory for Atomistic and Molecular Mechanics (LAMM), Department of Civil  
and Environmental Engineering, Massachusetts Institute of Technology, 77  
Massachusetts Ave., Cambridge, MA 02139, USA

<sup>4</sup>Center for Computational Engineering, Massachusetts Institute of Technology, 77  
Massachusetts Ave., Cambridge, MA 02139, USA

<sup>5</sup>Applied Mechanics and Structure Safety Key Laboratory of Sichuan Province,  
School of Mechanics and Engineering, Southwest Jiaotong University, Chengdu  
611756, China

\*Corresponding author, electronic addresses: [xuzp@tsinghua.edu.cn](mailto:xuzp@tsinghua.edu.cn)

This *Supplementary Material* contains

- Supplementary **Tables S1-S4, Figures S1-S4** and the captions
- Supplementary notes on the edge energy densities of 2D sheets

## I. Supplementary Tables, Figures and Captions

**Table S1** Tensile strength ( $\sigma_s$ ) of 2D materials and the adhesive strength ( $\gamma_i$ ) on specific substrates.

2D materials	$\sigma_s$ (N/m)	$\gamma_i$ (N/m)	Substrates
Graphene	36.014	1.204	Ni ( <a href="#">Xu and Buehler, 2010</a> )
		0.397	Cu ( <a href="#">Xu and Buehler, 2010</a> )
		0.345	Graphite ( <a href="#">Sen et al., 2010</a> )
		0.080	SiO <sub>2</sub> ( <a href="#">Sen et al., 2010</a> )
		0.020	PDMS ( <a href="#">Allen et al., 2009</a> )
Silicene	6.233	3.640	Bulk Si ( <a href="#">Stekolnikov et al., 2002</a> )
		1.350	Ag ( <a href="#">Qin et al., 2015</a> )
Germanene	4.294	2.640	Bulk Ge ( <a href="#">Stekolnikov et al., 2002</a> )
h-BN	24.910	0.130	Bulk BN ( <a href="#">Coleman et al., 2011</a> )
MoS <sub>2</sub>	15.301	0.304	Bulk MoS <sub>2</sub> ( <a href="#">Dolui et al., 2013</a> )
		0.240	H-terminated SiO <sub>2</sub> ( <a href="#">Dolui et al., 2013</a> )
		0.208	O-terminated SiO <sub>2</sub> ( <a href="#">Dolui et al., 2013</a> )
		0.140	Bulk MoS <sub>2</sub> ( <a href="#">Coleman et al., 2011</a> )
Black phosphorus	7.215	0.168	Black phosphorus ( <a href="#">Guan et al., 2014; Kim, 2014</a> )
Silica	36.787	3.022	Bulk silica ( <a href="#">Shchipalov, 2000</a> )
		0.513	Ru ( <a href="#">Loffler et al., 2010</a> )

**Table S2** Tensile strength ( $\sigma_s$ ) and adhesive strength ( $\gamma_i$ ) of typical scotch tapes.\*

Scotch Tape	$\sigma_s$ (N/m)	$\gamma_i$ (N/m)	Backing thickness (mm)
302	402	20	0.025
305	368	22	0.025
311	438	24	0.028
313	613	26	0.041
353	437	49	0.025
355	1174	85	0.051
369	333	32	0.025
371	385	44	0.03
372	455	49	0.035
373	525	55	0.041
375	613	60	0.051

\*Data is extracted from "3M-Scotch and Tartan Box Sealing Tape Guide",  
<http://www.trisupplies.net/Scotch-and-Tartan-Packing-Tape-Guide>, using  
American Standards for Testing of Materials (ASTM).

**Table S3** Mechanical parameters of typical 2D materials derived from first-principles calculation, which are used to construct the coarse-grained force field.

Materials	$K$ (N/m)	$D$ (eV)	$\nu$
Graphene	322.4	1.6	0.16
Silicene	59.7	0.37	0.28
MoS <sub>2</sub>	122.3	6.3	0.29
Silica	133.4	14.4	0.50

**Table S4** The coarse-grained force field developed for graphene, following the instruction described in Ruiz et al. (Ruiz et al., 2015).

Interaction terms	Functional forms	Parameters
Bond stretching	$D_0\{1-\exp[-A(d-d_0)]\}^2$ with a cut-off distance $d_c$	$d_0 = N_{CG} \times 1.4 \text{ \AA}$ $d_c = d_0 \times 1.16$ $D_0 = N_{CG}^2 \times 59.42 \text{ kcal/mol}$ $A = \ln(2)/(d_c - d_0)$
Angle bending	$k_\theta(\theta - \theta_0)^2$	$k_\theta = N_{CG}^2 \times 102.45 \text{ kcal/mol}$ $\theta_0 = 120^\circ$
Dihedral bending	$k_\phi[1 - \cos(2\phi)]$	$k_\phi = 4.15 \text{ kcal/mol}$

\* $N_{CG}$  is the coarse-grain degree in this force field.

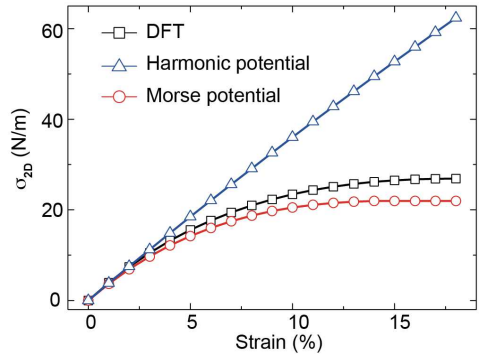


**Figure S1** Biaxial stress-strain relation calculated from DFT calculations, the harmonic approximation, and the Morse-type CG force field constructed in this work that captures the nonlinear behaviors.

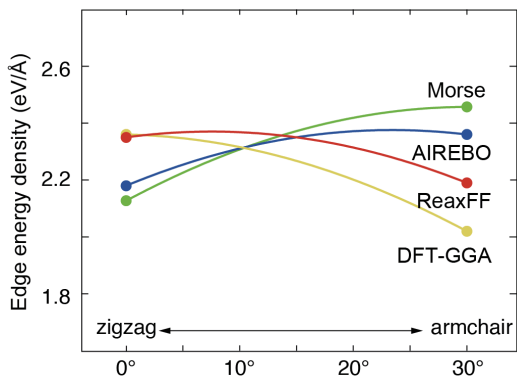


**Figure S2** The edge energy densities calculated using different models of interatomic interaction (dots) and those predicted from Eq. S1 (lines). The specific methods used to obtain the data are labeled: DFT calculations with general gradient approximation (GGA, the yellow line) (Liu et al., 2010), the AIREBO (Liu et al., 2010) or ReaxFF (Sen et al., 2010) potential based calculations, and the results derived from our Morse-type CG potential.

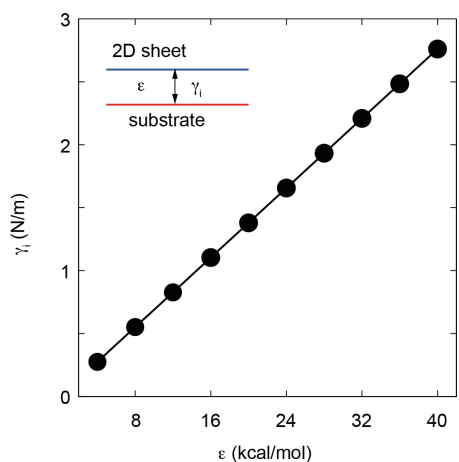


**Figure S3** Calibration of the adhesion strength  $\gamma_i$ , determined by the well depth  $\epsilon$  in 12-6 Lennard-Jones potential as implemented in the coarse-grained force field.

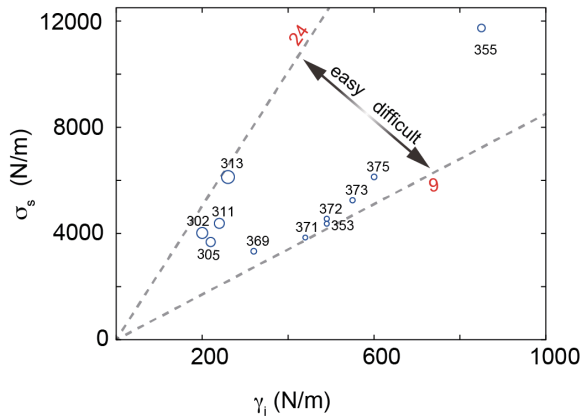


**Figure S4** The measured data of tensile strength ( $\sigma_s$ ) and adhesive strength ( $\gamma_i$ ) for scotch tapes (with types denoted in the plot, collected from references listed in **Table S2**), where the size of the data points indicates the ratio between the tensile strength and adhesive strength  $\sigma_s/\gamma_i$ . The dash lines define the upper and lower bounds of the ratio, which determines the feasibility for successful exfoliation of 2D materials.

## II. Supplementary Notes on the Edge Energy Density of 2D Sheets

The edge energy density quantifies the resistance to interatomic bond rupture. All bonds are equivalent in our coarse-grain model for the 2D sheets with a hexagonal lattice, and thus the edge energy density is proportional to the density of bonds cleaved as the crack advances for the same distance, which is higher for the more closely packed armchair edges than that for the zigzag edges, by a numeric factor of  $2/\sqrt{3}$ . The edge energy density for edges along arbitrary directions can then be fit through the equation formulated by Liu *et al.* ([Liu et al., 2010](#)) (**Fig. S2**).

$$\gamma(\chi) = |\gamma| \cos(\chi + C) \quad (\text{S1})$$

Here  $\chi$  is the chiral angle measured from the zigzag direction, and  $C$  is a phase shift constant characterizing the edge chemistry. It is worthy to note that, for some 2D materials such as graphene where the bond order in armchair edges could rearrange to form triple bonds and the edge energy density could be reduced to be even lower than that of the zigzag edge. The edge energy densities of armchair- and zigzag-type graphene edges calculated from DFT are 2.02 eV/Å and 2.36 eV/Å with a ratio of 1/1.17. Due to this fact, discussion involving the edge energies should be made with care.

## Supplementary References

- Allen, M.J., Tung, V.C., Gomez, L., Xu, Z., Chen, L.M., Nelson, K.S., Zhou, C.W., Kaner, R.B., Yang, Y., 2009. Soft transfer printing of chemically converted graphene. *Adv. Mater.* 21, 2098-2102.
- Coleman, J.N., Lotya, M., O'Neill, A., Bergin, S.D., King, P.J., Khan, U., Young, K., Gaucher, A., De, S., Smith, R.J., Shvets, I.V., Arora, S.K., Stanton, G., Kim, H.Y., Lee, K., Kim, G.T., Duesberg, G.S., Hallam, T., Boland, J.J., Wang, J.J., Donegan, J.F., Grunlan, J.C., Moriarty, G., Shmeliov, A., Nicholls, R.J., Perkins, J.M., Grieveson, E.M., Theuwissen, K., McComb, D.W., Nellist, P.D., Nicolosi, V., 2011. Two-dimensional nanosheets produced by liquid exfoliation of layered materials. *Science* 331, 568-571.
- Dolui, K., Rungger, I., Sanvito, S., 2013. Origin of the *n*-type and *p*-type conductivity of MoS<sub>2</sub> monolayers on a SiO<sub>2</sub> substrate. *Phys. Rev. B* 87, 165402.
- Guan, J., Zhu, Z., Tomanek, D., 2014. Phase coexistence and metal-insulator transition in few-layer phosphorene: A computational study. *Phys. Rev. Lett.* 113, 046804.
- Kim, H., 2014. Effect of van der waals interaction on the structural and cohesive properties of black phosphorus. *J. Korean Phys. Soc.* 64, 547-553.
- Liu, Y., Dobrinsky, A., Yakobson, B.I., 2010. Graphene edge from armchair to zigzag: The origins of nanotube chirality? *Phys. Rev. Lett.* 105, 235502.
- Löffler, D., Uhlrich, J.J., Baron, M., Yang, B., Yu, X., Lichtenstein, L., Heinke, L., Buchner, C., Heyde, M., Shaikhutdinov, S., Freund, H.J., Włodarczyk, R., Sierka, M., Sauer, J., 2010. Growth and structure of crystalline silica sheet on Ru(0001). *Phys. Rev. Lett.* 105, 146104.
- Qin, Z., Xu, Z., Buehler, M.J., 2015. Peeling silicene from model silver substrates in molecular dynamics simulations. *J. Appl. Mech.* 82, 101003.
- Ruiz, L., Xia, W.J., Meng, Z.X., Keten, S., 2015. A coarse-grained model for the mechanical behavior of multi-layer graphene. *Carbon* 82, 103-115.

Sen, D., Novoselov, K.S., Reis, P.M., Buehler, M.J., 2010. Tearing graphene sheets from adhesive substrates produces tapered nanoribbons. *Small* 6, 1108-1116.

Shchipalov, Y.K., 2000. Surface energy of crystalline and vitreous silica. *Glass Ceram.* 57, 374-377.

Stekolnikov, A.A., Furthmuller, J., Bechstedt, F., 2002. Absolute surface energies of group-iv semiconductors: Dependence on orientation and reconstruction. *Phys. Rev. B* 65, 115318.

Xu, Z., Buehler, M.J., 2010. Interface structure and mechanics between graphene and metal substrates: A first-principles study. *J Phys. Condens. Matter* 22, 485301.